Final report

Title of the project:

"Innovative cryogenic diode laser bars optimized for emerging ultra-high power laser applications" (CryoLaser)

EXECUTIVE SUMMARY

<u>Goals</u>

Diode lasers have been the key elements in high power laser systems for decades. A new generation of ultra-high power systems based on diode laser technology is in construction and planning world-wide. These systems are performing the research and development work needed to enable the eventual introduction of laser-induced fusion as a clean, safe, highly efficient power source, as well as performing basic research. Although prototype systems are possible with today's technology, a new kind of diode lasers with drastically increased power density, efficiency and reduced spectral width is required for realistic laser-induced fusion systems. The goal of the CryoLaser project was to meet this need. The objectives were to increase the emitted optical output power density by a factor of ~10 and to increase the power conversion efficiency at the operation point to > 80% (reducing the dissipated heat threefold). Also, internal gratings were introduced into the diode lasers, for increased pumping efficiency. These improvements were to be achieved by developing innovative device designs for use at sub-zero (200 K) temperatures.

<u>Methods</u>

Within the CryoLaser project, the FBH developed the infrastructure necessary for the design optimization of high power diode lasers for sub-zero temperatures, including new and improved simulation and design tools and fabrication and mounting technology for diode laser bars and stacks, as well as the installation of test facilities at 200 K for verification of the results. The new infrastructure was used to design, construct and assess the performance of novel diode laser designs with high precision to the highest powers and currents. Multiple design iterations were performed, to understand and address the limits to performance. All research, technology development and prototype construction of diode lasers was performed at the FBH. However, in order to ensure that the technology developed is suitable for later transfer into real systems, the studies within CryoLaser were performed in cooperation with the world leading groups involved in developing laser-induced fusion (Lawrence Livermore national labs in the USA and STFC in the UK, supported by HiLASE in the Czech Republic). These partners assessed prototypes from the FBH and helped develop a joint strategy for diode lasers for ultra-high power laser systems.

<u>Results</u>

Low temperature operation of around 200 K and the use of custom epitaxial, process and packaging designs enabled diode laser bar conversion efficiency at 400 W to be increased to 77%, the highest efficiency ever reported from a laser bar, and close to the targeted 80%. Also, conversion efficiency of 70% (similar to the best commercial bars) can be achieved at a much higher power level per bar of 1000 W (compared to 400 W commercial). Finally, operation at 1600 W per bar (at 60% efficiency) has been confirmed and up to 2000 W demonstrated, confirming a > 10x increase in optical power density. However, diode lasers with monolithically integrated gratings showed reduced efficiency and require additional development. The reported results were confirmed via testing of prototype diode lasers by the project partners. Although below the project targets, this represents substantial performance improvement over the current state of the art and the results from CryoLaser are anticipated to enable a large reduction in cost in €/W of the diode laser pump sources for large laser facilities. In addition, important new understanding on the limits to conversion efficiency in diode lasers has been obtained, with (for example) significant excess electrical resistance being traced to limitations to injection into the active region. CryoLaser delivered significant scientific impact, producing 20 technical papers and conference presentations (8 invited), two bachelor, one masters and one PhD thesis. The technology developed in CryoLaser has helped enable the FBH's industrial partners to deliver the first commercial kilowatt-class diode laser bars for room temperature systems, and forms the basis for several follow-on projects.

2

TABLE OF CONTENTS

A: MOTIVATION

Multi-joule high-energy-class solid state laser systems are a key emerging technology, with large laser facilities planned or constructed worldwide, such as NIF, ELI, HiLASE and Laser Megajoule. These facilities deliver extremely high intensity coherent optical energy (~10…1000 J, compressed to femotoseconds for Petawatt-class peak powers) for fundamental studies in physics and material science. Such high energy pulses also potentially enable whole new fields of commercial applications, up to and including power generation via laser-induced fusion. The optical energy delivered by these laser systems is generated via optical power amplification of a seed pulse, and the achievable output energy, conversion efficiency and repetition rate are mainly limited by the performance of the amplifiers and their optical pumps. Specifically, pump sources with the very highest output power and conversion efficiency are needed for next generation systems, and such sources do not exist. The goal of the CryoLaser project was to change this.

B: PROJECT GOALS

Although diode lasers are the most efficient and highest power pump sources, their performance is lower than needed for next-generation systems. The amplifier crystals in many high-energy-class lasers are cooled to temperatures of ~150 K, meaning that cryogenic cooling of the diode laser pumps is also feasible. Therefore, custom diode laser designs and technology were developed within the CryoLaser project that leverage the improved semiconductor properties at operating temperatures around 200 K to enable a step improvement in diode laser performance. Specifically, ultra-high power and efficiency diode lasers were to be designed, fabricated and delivered to key users in the high energy laser community. These novel bars targeted an operation power at heat sink temperature T_{HS} = 200 K of P_{op} = 1600 W for per-bar optical power density I = 107 kW/cm^2 (~ 10x higher than state of the art in 2011) at a power conversion efficiency at the operating point of η_E (P_{op}) ~80% (2011 state of the art: 60%). Pumping efficiency was to be increased by the implementation of a wavelength stabilizing monolithically integrated grating. Finally, 5 bars were to be stacked into a high density stack to deliver higher total powers from a single low-cost package whilst sustaining I > 100 kW/cm². Targeted wavelengths were 940 nm and 872 nm, for pumping the most widely used solid state gain media, Yb:YAG and Nd:YAG respectively. Results and example devices were shared, and development strategy discussed trough the project with the leading groups developing laser-induced fusion systems, namely the Central Laser Facility (part of the STFC) in the UK and the Lawrence Livermore National labs in the USA.

C: SUMMARY OF RESULTS ACHIEVED IN EACH WORK PACKAGE

The efforts within CryoLaser were divided into four work packages: Simulation, Design, Manufacturing and Characterization, which developed the tools needed to design, realize and precisely and accurately assess performance of high power diode laser bars tailored for 200 K operation. The results achieved in each work package are summarized below.

WP1: SIMULATION

Available FBH simulation tools were expanded to include operation temperatures down to 200 K, building on a detailed characterization of the material properties of FBH semiconductor layers and characteristic parameters of exemplary diode lasers.

C1.1 Material parameters - electrical

First, a series of $Al_xGa_{1-x}As$ bulk-layer test samples were epitaxially grown on semi-insulating substrates with a wide range of Al-content (x=0…85%) and n- and p-type doping levels ($3 \times 10^{16}…1 \times 10^{18}$cm^{-3}). The range covered all compositions anticipated for use in high power

4

diode lasers tailored for high-power operation at low-temperatures. The carrier concentration as well as carrier mobility of the test samples was measured as a function of temperature in the range 15 K – 300 K using by Hall measurements, following standard practice. The carrier density and mobility were determined at each temperature, and used to derive ionization energies of the carriers. Furthermore, material conductivity was determined and compared to literature. Results are described in detail in [A]. Example test data for electron and hole mobility for some selected samples is shown in Figs 1 and 2, compared to a generalized fit function taken from Sotoodeh *et al.*[1] Overall, high bulk mobility and low ionization energy were observed across the whole design range of 200…300 K. The characteristics of the most critical (lowest mobility) p-type material could be well reproduced using the generalized fit function. For both n- and p-type doping, the ionization energies were low and no significant carrier freeze out was observed in the 200-300 K range for the critical waveguide layers. Therefore, the bulk-layer resistance is expected to reduce as temperature falls, due to increased mobility. The fit functions shown in Figs. 1 and 2 were used later in full device simulation in the FBH tools QIP and WIAS-TESCA to estimate the performance expected as a function of temperature of various diode laser designs.
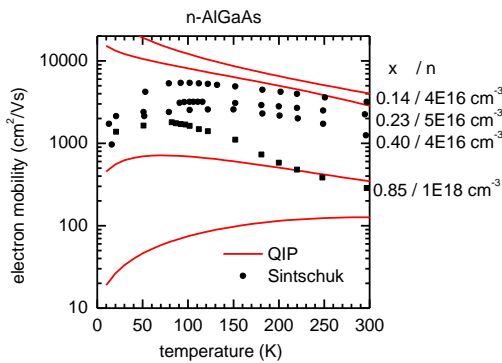

Fig. 1: Measured electron mobility as a function of temperature (points) for a range of n-doped bulk AlGaAs sample, compared to the results of a generalized fit function (lines). Although absolute values differ significantly, the temperature dependence is reproduced.
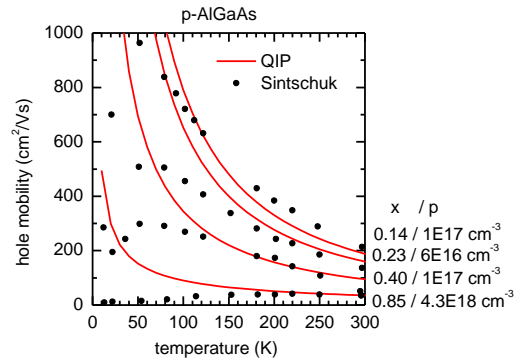
Fig. 2: Measured hole mobility as a function of temperature (points) for a range of p-doped bulk AlGaAs sample, compared to the results of a generalized fit function (lines). Although absolute values differ marginally, the temperature dependence is reproduced.

C1.2 Material parameters – optical

As a second step, the development of characteristic diode laser parameters was studied as a function of temperature. An example diode laser design was selected, and a series of test devices with different resonator length, L, fabricated, bonded and tested, as described in detail in [5,19]. The resonator-length-dependence of threshold current and slope was used to assess the temperature dependence of internal optical loss α_i, internal differential efficiency η_i, modal gain parameter Γg_0 and transparency current density J_{transp}. As shown in Fig. 3, α_i was found to be only weakly temperature dependent down to 200 K, whilst η_i increased, consistent with the freeze out of carrier loss mechanisms such as leakage and Shockley-Read-Hall recombination, as discussed in [5,19]. Also as shown in Fig. 3, the lasing wavelength varied with temperature at a consistent rate of 0.34 nm/K. The temperature variation of Γg_0 and J_{transp} will be discussed in later sections. Please note: the error bars in Fig. 3 indicate the accuracy of fit to the length dependence, as discussed in [19].

---

[1] M. Sotoodeh, A. H. Khalid and A. A. Rezazadeh, J. Appl. Phys. 87(6), p. 2890 (2000).
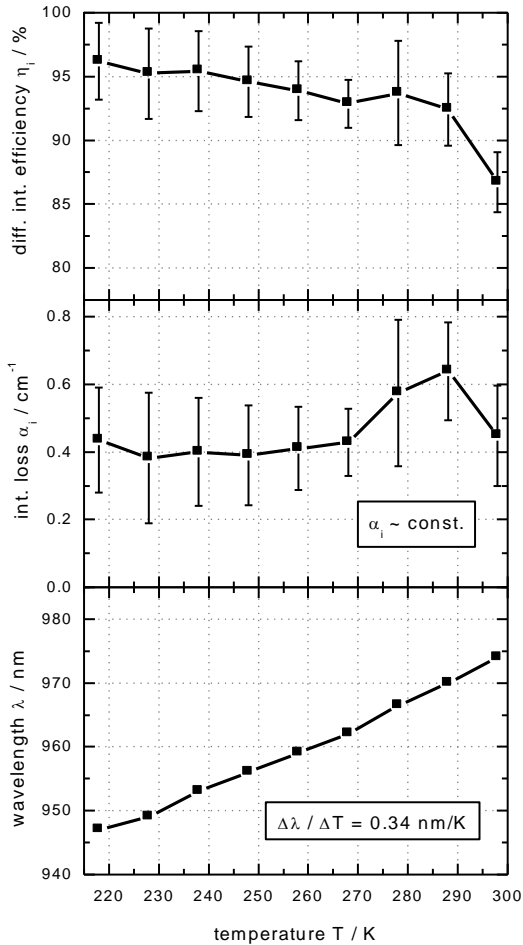
Fig. 3: Differential internal efficiency (top), internal loss (middle) and centroid wavelength (bottom) vs. temperature for exemplary diode lasers with 100 μm stripe width [19].
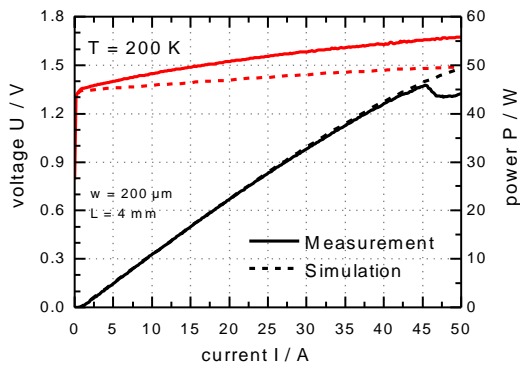

Fig. 4: Voltage (red) and power (black) vs. current. Measured values (solid) from a 200 μm wide single emitter lasing at $\lambda = 975$ nm are compared to WIAS-TESCA simulations (dashed). The power-current characteristic is well reproduced (excepting a kink at 45 A), but not current-voltage.

C1.3 Implementation into simulation tools

Experimental information on the temperature dependence of electrical and optical properties was used as input to develop full self-consistent laser simulation, following the approach of Wenzel *et al.*[2], adapted for low temperature operation. Specifically, the extracted parameters were implemented into the simulation tools FBH-QIP and WIAS-TESCA. Full laser simulation using WIAS-TESCA showed good agreement with measured diode laser chips at 200 K in the current-power characteristic, as shown in Fig. 4 for an example diode laser with stripe width $W = 200$ μm and resonator length $L = 4$ mm mounted junction down on CuW carrier. The device was tested under quasi-continuous wave (QCW) conditions, with pulse width $\tau = 1.2$ ms and repetition rate $\nu = 10$ Hz. However, there still remained a significant difference in the current-voltage characteristic, as discussed later. Subsequent vertical design development was performed using the 1D diode laser design tool FBH-QIP, now taking into account temperature dependence device parameters.

WP2: VERTICAL DESIGNS

C2.1 It. 1: Assessment of limiting factors

The influence of vertical (epitaxial layer) design was studied in WP 2 and novel designs were sought with improved performance. As a first step, to help direct the design studies, the relative influence of key device performance characteristics on conversion efficiency at higher powers was analyzed for an example FBH structure. Figs. 5-7 illustrate the influence of variation in threshold current, optical loss and series resistance, R_s, on efficiency at 20 W output power, for example diode lasers operating at a wavelength $\lambda = 940$ nm and $T_{HS} = 300$ K with $W = 100$ μm and $L = 4$ mm ($\tau = 1.2$ ms, $\nu = 10$ Hz). The analysis

---

[2] H. Wenzel *et al. New Journal of Physics* 12, p. 085007 (2010)

revealed that R_s has the biggest influence on efficiency at $P_{op} = 20W$, followed by the slope efficiency (here varied using the internal optical loss).

Therefore design development was performed by adapting established FBH structures to achieve lower R_s without degrading the slope efficiency (i.e. maintaining low internal optical losses as well as high internal efficiency). Here, the waveguide layers proved to be crucial, as they were predicted to be responsible for most of the series resistance and optical loss [4]. R_s is influenced by the thickness of the waveguide, its asymmetry, the doping and the material composition. Increasing the doping in the waveguide was not an option as this leads to higher optical losses.
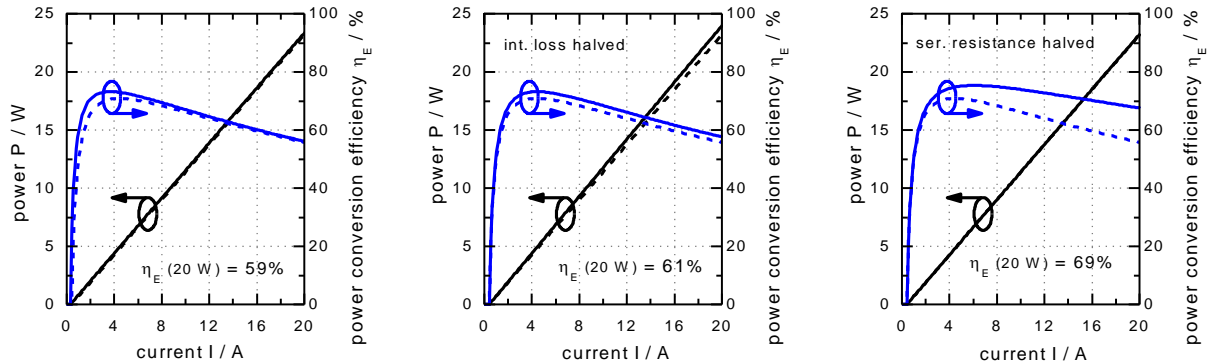
Power (black) and efficiency (blue) vs. current. Extrapolated performance is shown (solid), compared to a reference device (dashed).

| Fig. 5: Threshold current is artificially lowered by 30%, resulting in only a small increase in efficiency at 20 W to 59%. | Fig. 6: Internal loss is artificially lowered by 50%, resulting in a moderate increase in efficiency at 20 W to 61%. | Fig. 7: Series resistance is artificially lowered by 50%, resulting in a strong increase in efficiency at 20 W to 69%. |

C2.2 Iteration 2: Low-Al-content designs

As a second step, a series of vertical laser designs was designed and fabricated, to experimentally study options for lower resistance, focusing on the impact of material composition. Specifically, a baseline structure with a 2.4 µm thick $Al_xGa_{1-x}As$ waveguide and a single quantum well emitting at $\lambda = 975$ nm was used to investigate the influence of the Al-content on the power and voltage characteristic at different temperatures. As confirmed in the studies in WP 1, reducing the Al-content, x, of the $Al_xGa_{1-x}As$ layers increases carrier mobility, which leads to lower R_s. However, the barrier heights around the active region simultaneously decrease, leading to deteriorated electrical confinement of carriers in the quantum well, which degrades performance. FBH-QIP was used to define a series of structures, where the Al-content of the waveguide and n-side cladding layers was stepwise reduced. The expected R_s for the bulk layers used in the design was extracted, based on the fit functions obtained in WP1, and combined with an estimate of contact and substrate resistance to yield total expected chip resistance. The conduction and valence band edges of selected examplary vertical structures are shown in Fig. 7, and the calculated R_s and quantum well depth ΔE are shown in Table 1 (ΔE is the difference between the conduction band edge for the waveguide layers and the energy of the first confined electron state in the well, see [5,19]). A significant decrease in series resistance was extrapolated (reduced from 14…10 mΩ).

Higher order modes in these structures were suppressed by tailoring the n-cladding composition for high optical losses for all but the fundamental mode. All heterojunctions (e.g. cladding-waveguide, waveguide-active region) were graded (GRIN) to facilitate carrier transport and avoid

7

sharp steps in the band profile, which could add to R_s. The designs were grown and processed to produce diode lasers, using a simplified, fast turn-around "short loop" process, modified to enable p-up packaging. After facet coating, example chips were mounted p-up on CuW carriers and tested under QCW conditions (τ = 1.2 ms, ν = 10 Hz) as a function of temperature using the test stations produced in WP4. The low energy barriers around the quantum well caused significant deterioration of the performance at room temperature, but waveguides with Al-content as low as x = 4% showed comparable optical performance at T_{HS} = 220 K to designs with x = 15% (used at T_{HS} = 300 K). A comparison of two key device parameters (η_i and J_{transp}) is shown in Table 2 for x = 4% and 15%, and their variation with temperature is shown in Fig. 8 (plotted as function of barrier height, scaled by the thermal energy $k_B T_{HS}$). Since both the transparency current density as well as the differential internal efficiency show strong exponential behavior in the case of low energy barriers, this was attributed to thermal leakage of carriers out of the quantum well. For higher barriers, η_i and J_{transp} saturate. Plotting the two variables against each other, as shown in Fig. 9, reveals a consistent trend for all structures (with and without leakage), suggesting that reducing the transparency current density will in general lead to increased differential efficiency [19]. A further key trend was observed in the same data series, as discussed in detail in [19]: measured R_s is significantly larger than predicted from the bulk layer mobility and increases as the effective barrier height $\Delta E/k_B T_{HS}$ rises, i.e. R_s increases as temperature falls, opposite to the trend in the mobility and bulk layer resistance, which fall. This is an important new observation, indicating that there is a significant electrical resistance associated with injection into the active region.

Full laser bars were fabricated to a selected number of these designs in WP3 and tested in WP4, where key results are summarized. Specifically, designs with waveguides in the range x = 4-7.5% were selected for use at T_{HS} = 200 K, because x = 0% shows degraded performance. However, it should be noted that when an aluminum content of 4% is used in the waveguide, (although resistance is low), power and efficiency at high bias were found to be limited by bias-induced leakage effects similar to those described in Wang *et al.*[3]

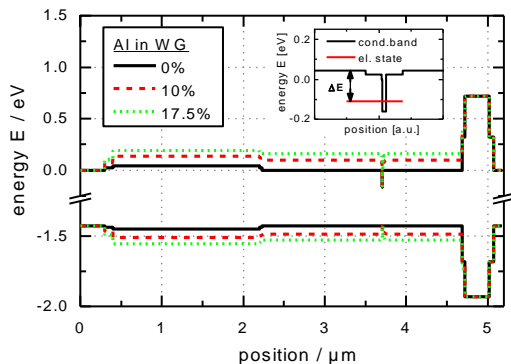| Al [%]	R_S [mΩ]	ΔE [meV]
0	10.3	91
4	10.9	127
7.5	11.5	171
10	12.0	193
12.5	12.7	213
15	13.1	235
17.5	14.0	252

Fig. 7: Calculated conduction and valence band edges as a function of depth for laser designs with different Al-contents in the waveguide (0% - solid, 10% - dashed, 17.5% - dotted). Inset: Example barrier height ΔE around the quantum well.

Table 1: Calculated values for structures with different Al-content in the waveguide for a 4 mm long, 100 µm wide single emitter.

C2.3 Iteration 3: Vertical layer optimization

A second design iteration was then performed, seeking further improved efficiency. The waveguide thickness was reduced from 2.4 µm to 1.3 µm, increasing confinement factor,

[3] X. Wang *et al.*, IEEE J. Quantum Electron. 46(5), p. 658 (2010).

targeting reduced threshold current. The doping profile and asymmetry of the vertical waveguide was also fine-tuned, lowering α_i from 0.4 cm^{-1} to 0.3 cm^{-1}. The use of thin, asymmetric vertical waveguide allowed higher aluminum content to be used for the waveguide without compromising series resistance, minimizing high-bias leakage effects. A comparable design with $x = 15\%$ for the waveguide was also assessed, as a baseline structure. Optical performance parameters were derived from measuring multiple devices with different resonator lengths at room temperature and the results of this analysis are shown in table 3. The measured modal gain increased as expected, but less than anticipated.

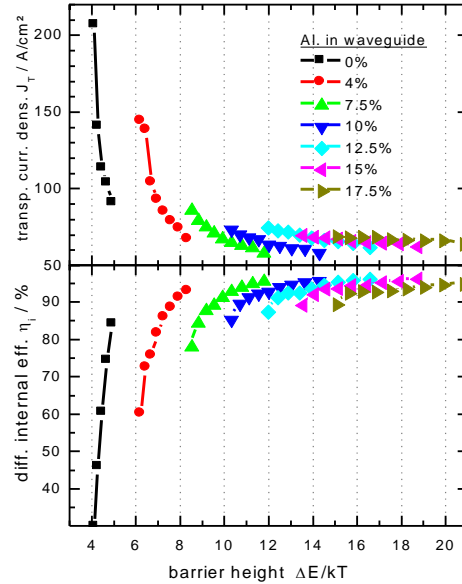|	4% Al.	15% Al.
J_{transp} (290 K) [A/cm²]	144	70
J_{transp} (220 K) [A/cm²]	67	63
η_i (290 K)	60%	90%
η_i (220 K)	93%	94%

Table 2: Transparency current density and differential internal efficiency at $T_{HS} = 290$ K and 220 K for two structures with different Al-content in the waveguide.

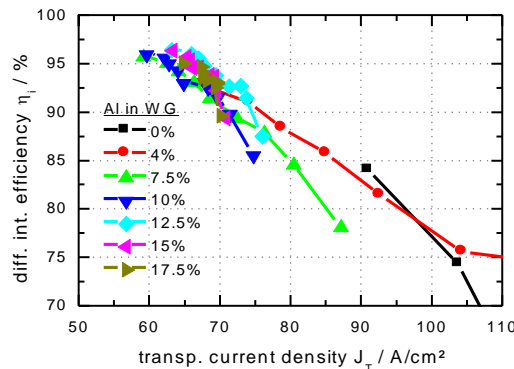Fig. 8: Transparency current density and differential internal efficiency vs. barrier height $\Delta E/kT$.

Fig. 9: Differential internal efficiency vs. transparency current density as extracted from Fig. 8.

In parallel, in a third design, the quantum well was modified to support lasing at $\lambda = 870$ nm at $T_{HS} = 200$ K (as needed to pump Nd-doped solid state media). The vertical design was adjusted, increasing the aluminum content of waveguide layers to provide sufficient barriers against carrier leakage from the active region, for anticipated performance close to that for designs with $\lambda = 975$ nm at $T_{HS} = 200$ K.

C2.4 Lateral current spreading

As noted earlier in WP1, at low temperatures the carrier mobility increases and this will lead to increased lateral current spreading. Current spreading leads to carrier losses at the device

edges, as reported by Smowton et al.[4], and could significantly reduce conversion efficiency. To assess if this plays a limiting role, the width of the optical field on the output facet was measured as a function of heatsink temperature and output power, using newly constructed test equipment, as described later in WP4. As shown in Figs 10, 11, no significant increase was observed in the width of the optical field, which we take as evidence that current spreading plays only a small role.
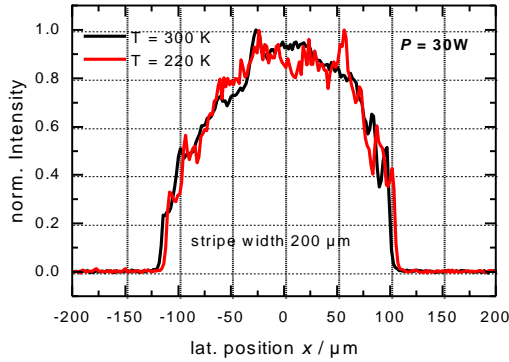
Fig. 10: Lateral near field profile of a 200 μm wide single emitter at a power of 30 W at temperatures of 300 K (black) and 220 K (red).
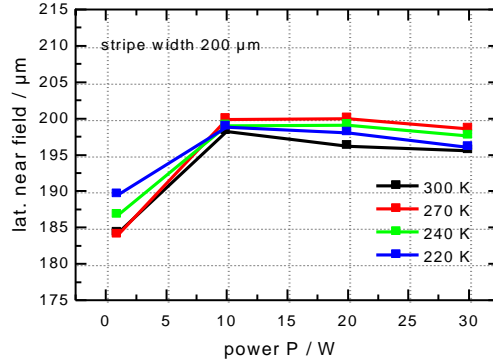
Fig. 11: Development of the lateral near field for a 200 μm wide emitter with output power for four different temperatures (300 K – black, 270 K – red, 240 K – green, 220 K – blue).

	4% Al. It. 2	7.5% Al. It. 3
R_S [mΩ]	13	13
ΔE [meV]	127	166
η_i	74%	84%
Γg_0 [cm^{-1}]	7.5	8.5
J_{transp} [A/cm²]	130	137
α_i [cm^{-1}]	0.4	0.3

Table 3: Measured device performance parameters for designs from It. 2 and It. 3 at T_{HS} = 290 K. While series resistance is unchanged, optical loss, barrier height and modal gain parameter are improved.

C2.5 Implementation of monolithically integrated gratings

The Yb-doped gain media used in high-energy class solid state amplifiers are most efficiently pumped by sources with narrow spectral lines $\Delta\lambda_{95\%}$ < 1 nm (95% power content), much smaller than the normal lasing linewidth of diode lasers, $\Delta\lambda_{95\%}$ ~ 6…8 nm, as reported by Ertel et al.[5] Wavelength narrowing using external gratings adds substantial cost, so monolithically integrated gratings would be very attractive, for efficient pumping at lowest cost in €/W. Therefore, grating technology developed at the FBH in previous research programs was assessed for use in high power bars. Diode lasers with uniform distributed feedback (DFB lasers) were fabricated using two alternative grating technologies: either by (a) etching periodic grooves into the surface of a completed epitaxial structure or (b) by halting the growth, etching a grating then completing the vertical structure with a second growth stage. In previous studies, overgrown DFB gratings produced by the FBH operated with negligible additional losses as reported by Schultz et al.[6] However, during the CryoLaser project (in spite of the use of a patented in-situ cleaning process that had previously operated very successfully) high levels of oxygen were incorporated into the epitaxial structure when re-growth was performed. The final diode lasers then operated with strongly reduced η_i.

[4] P. M. Smowton and P. Blood, Appl. Phys. Lett. 70(9), p. 1073 (1997).

[5] K. Ertel et al. Optics Express 19(27), p. 26610 (2011).

[6] C.M. Schultz et al., Appl. Phys. Lett. 100, p. 201115 (2012).

The oxygen incorporation was correlated to the quality of the chemical surface cleaning used before re-growth started, but no solution could be found within the duration of the CryoLaser project. Operating at low heat sink temperatures did not suppress the efficiency loss seen in DFB lasers with overgrown gratings, as can be seen in Fig. 12, although the spectrum was narrowed successfully. In parallel to CryoLaser, the BRIDLE project (www.bridle.eu) performed technology development on DFB lasers with surface etched gratings. However, the most advanced configuration available for CryoLaser introduced an additional optical loss of 0.3 cm^{-1}, so was unsuitable for high efficiency operation, as reported by Decker *et al.*[7] Therefore, both surface and overgrown gratings lead to reduced efficiency so were not suitable for use within CryoLaser. Further studies are necessary, but were outside the scope of the project.
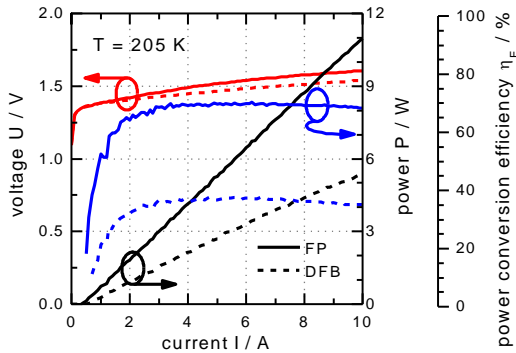

Fig. 12: Power (black), voltage (red) and efficiency (blue) vs. current for a reference Fabry-Perot device (solid) and a device with an overgrown DFB grating (dashed).
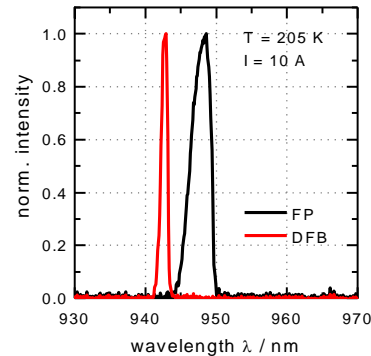
Fig. 13: Spectrum at a current of 10 A of the reference Fabry-Perot device (black) and the DFB device (red). The DFB device operates at λ = 942 nm, with $\Delta\lambda_{95\%}$ < 1 nm.

WP3: PRODUCTION / ASSEMBLY

C3.1 Development in epitaxial growth techniques

The epitaxial designs developed for low temperature operation discussed in WP2 incorporated low Al-content (with composition graded controllably down to 0%) and low doped layers (controllably regulated to around a few 10^{16} cm^{-3}). The epitaxial growth reactors at the FBH were successfully upgraded to be able to controllably and reproducibly realize such structures.

C3.2 Lateral Processing

The designs developed in WP2 were epitaxially grown at the FBH and subsequently processed in one of two process types. First, in a simplified, low cycle-time "short-loop" process, broad area diode lasers with various cavity lengths are rapidly fabricated, allowing their characteristic parameters to be determined by measuring (with 1 µs current pulses) a series of unmounted diode lasers with different cavity lengths. During the course of the project this process was upgraded with an improved n-side metallization, to allow single emitters from the processed wafers to be packaged (p-up) and tested as a function of temperature, although the peak achievable power is limited to ~ 10 W. Many such cycles were performed, with the most important results presented here. Second, wafers with pre-tested and established designs were fabricated into single emitters of different lengths and widths and into bars with high fill factors, using a full technological process suitable for operation to the highest output powers. Three such full processes were completed (Iterations 1-3) during the course of the project, in each case assessing a series of new epitaxial designs. Two bar (lateral) designs were developed during CryoLaser, one with 37 x 186 µm stripes for a fill factor of 69% and one with fewer, wider stripes, namely 18 x 400 µm (fill factor 72%), both available with *L* = 4 or 6 mm, as shown schematically

[7] J. Decker *et al.*, IEEE Photon. Technol. Lett. 27(15), p. 1675 (2015).

11

in Fig. 14. Technological development was necessary and successfully realized, to increase the number of diode lasers included in each bar (increase in fill factor), without introducing process defects. The configuration with 400 µm wide stripes sub-divided each electrical contact into periodically pumped and un-pumped sub-stripes, in order to suppress ring lasing. In all cases, the stripe width was defined by implantation of the contact layer and lateral guides were etched to provide a refractive index change for lateral optical confinement (nominal change in effective refractive index $\Delta n_{eff} = 10^{-3}$). Studies were also performed for a backside / n-metallization which allows the direct soldering of bar onto bar (see section 3.5).
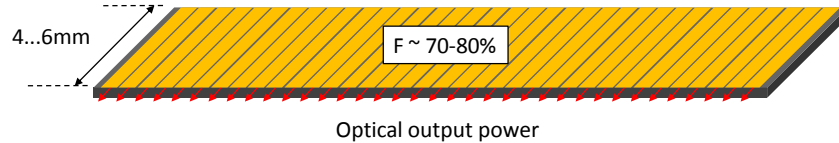

Fig. 14: Schematic drawing of a high fill-factor bar

C3.3 Facets

Once lateral processing was finished, diode bars were cleaved from the wafer and their facets were treated. In a first step the facets were passivated using ZnSe, as described by Ressel *et al.*[8], inhibiting catastrophic optical mirror damage. Coating of the facets with dielectric layers (antireflection for front facet, high reflection for rear facet) provides the optical feedback for lasing, with reflectivities chosen for maximum conversion efficiency, and to suppress higher-order vertical modes, if necessary, following the approach of Crump *et al.*[9]

C3.4 Mounting / Assembly

A new mounting scheme was developed to support the high currents and provide good cooling to the bars. The semiconductor chips were soldered between two CuW heatspreaders with AuSn and the sandwich was mounted p-side down onto a conduction cooled package (CCP) with indium. In a first iteration, the n-contact was established via a Cu-foil which enabled the assembly and kA-class test of bars with $L = 2…6$ mm. However, it was later experimentally discovered that the Cu-foil added series resistance close to that of the bar itself, limiting efficiency and power. A new mounting scheme was therefore developed in which a massive Cu-block served as the n-contact, both eliminating packaging resistance R_p as an efficiency limit (R_p reduced from ~ 200 µΩ to ~ 10 µΩ) and providing additional cooling from the n-side, limiting roll-over of the output power characteristic. The two packaging styles are shown in Fig. 15, and the impact on optical performance is shown in Fig. 16 ($T_{HS} = 200$ K, $\tau = 0.2$ ms, $\nu = 10$ Hz).
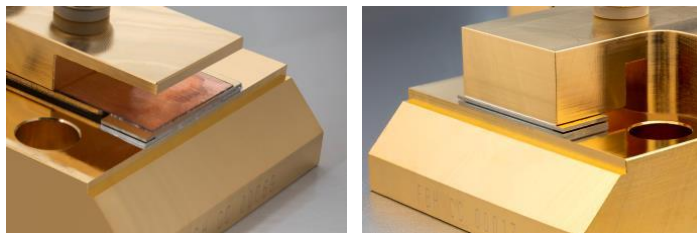

Fig. 15: Bars mounted on a CCP using a copper foil (left) and a massive Cu-block (right) as the n-side contact.
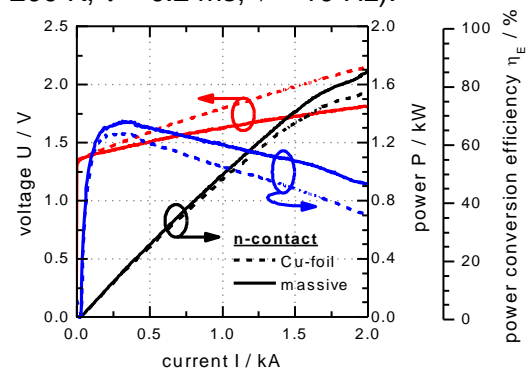
Fig. 16: Power (black), voltage (red) and efficiency (blue) vs. current for identical bars with different n-contacts.

[8] P. Ressel *et al.*, IEEE Photon. Technol. Lett. 17(5), p. 962 (2005).
[9] P. Crump *et al.*, Electron. Lett. 45(1), p. 51 (2009).

C3.5 High density (HD) stacks

As discussed by Feeler *et al.*[10], a potential technique for lowering the cost of large pump arrays in €/W is to solder the diode laser bars directly onto each other to form a vertically high density (HD) stack, simplifying assembly and saving significantly on component costs. The approach followed was to deposit patterned AuGe onto the n-side of the complete processed laser wafers. Five cleaved bars were then stacked directly on top of each other into a frame, all elements pressed together by springs and facet passivated and subsequently coated. During facet passivation and coating, high enough temperature were achieved for the bars to be soldered together. The high melting temperature of AuGe solder joint meant that the five bar stack could subsequently be soldered between CuW carriers with AuSn solder as a single building block, before being attached to CCP for measurements. The high melting point of the AuGe solder also limited out-diffusion during facet passivation, preventing any potential contamination of the facets. Substantial technological development was performed, as described in [B], with solder trials showing that altered n-side metallization, a custom deposition mask and a custom n-side sputter deposition were necessary to achieve a good bond and to avoid short circuits. A technological recipe was derived based on these studies and used in the second full laser process. The HD-stacks however showed degraded performance on testing, as shown in Fig. 17 at T_{HS} = 200 K (τ = 0.2 ms, ν = 10 Hz), along with a photo of a completed HD-stack. Although 5 bars were driven in series, power did not increase five-fold compared to a single bar. A possible reason for the power loss is the inhomogeneous power distribution across the stack, as shown in the intensity map in Fig. 18, which suggests that different emitters are not correctly contacted or are subjected to different drive currents. Therefore, due to the low performance and low yield, no deliveries of HD stacks were made to the project partners. Further development efforts are needed which were outside the scope of the project.
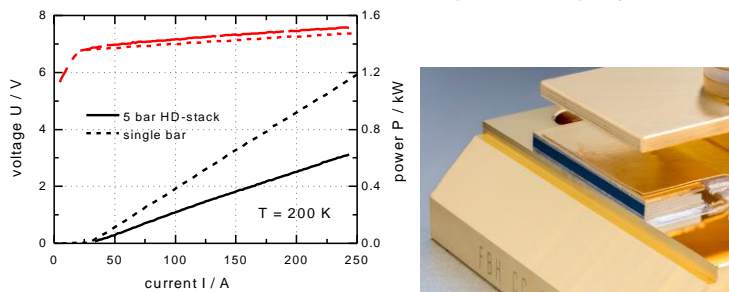

Fig. 17: (Left) Voltage (red) and power (black) vs. current for a 5 bar HD-stack (solid) and a single bar (dashed) scaled by a factor of 5. (Right) Photo of an complete assembled HD stack.
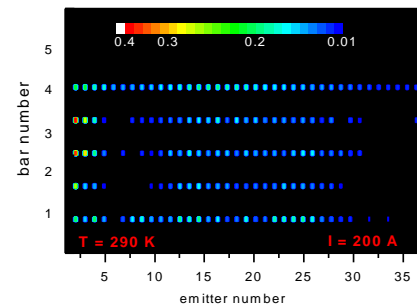

Fig. 18: Power distribution over a 5 bar HD-stack at 200 A and T_{HS} = 300 K. An inhomogeneous power level is seen.

WP4: MEASUREMENTS

For the measurements of fully assembled diodes (single emitters, single bars, stacks), two test stations were designed and carefully calibrated in WP4.

C4.1 Construction and calibration of test stations

The backbone of both stations consisted of a metal single walled vacuum chamber encased in insulation in which the diode was placed onto a temperature controlled heatsink. The light was extracted via an anti-reflection coated window so that the optical measurements could be

---

[10] R. Feeler *et al.*, Proc. SPIE 7916, 791608 (2011).

performed outside of the chamber at room temperature. Cooling was performed using silicon oil, which was pumped in a closed loop from a chiller to the laser heatsink. The temperature was measured by a sensor in the heatsink, and controlled via an integrated PID controller in the chiller. Within the chamber, current was supplied via thick copper flat band cables for minimum inductance and voltage was measured in an Ohmic configuration. Various current supplies were used for single emitters and bars, with bars driven using a custom 2 kA-QCW current supply developed in close coordination with the manufacturer, Amtron. The current was measured via an in-line resistor. All devices were measured under QCW conditions, with single emitters tested with $\tau = 1.2$ ms and $\nu = 10$ Hz, and bars tested under the appropriate conditions for the targeted solid state amplifier material, namely $\tau = 1.2$ ms and $\nu = 10$ Hz for diode lasers with $\lambda = 940…975$ nm (pumping Yb-doped media) and $\tau = 0.2$ ms and $\nu = 10$ Hz for diode lasers with $\lambda = 870…900$ nm (pumping Nd-doped media), unless stated otherwise. The first test station was used for determining the power-voltage-current (PUI) and spectral characteristics of the diodes. The light exiting the chamber through the window was collected in a customized integrating sphere. Attached to the sphere were a thermoelectric detector for wavelength-insensitive average power measurement, a fast photo diode for pulse shape determination and an optical fiber leading to a spectrometer. Careful calibration of the system (especially measurements of power, compared to absolute standards [6]) guaranteed reproducible and very accurate characterization of the diodes. Fig. 19 shows a schematic cross section and Fig 20 shows a photo of the test station.

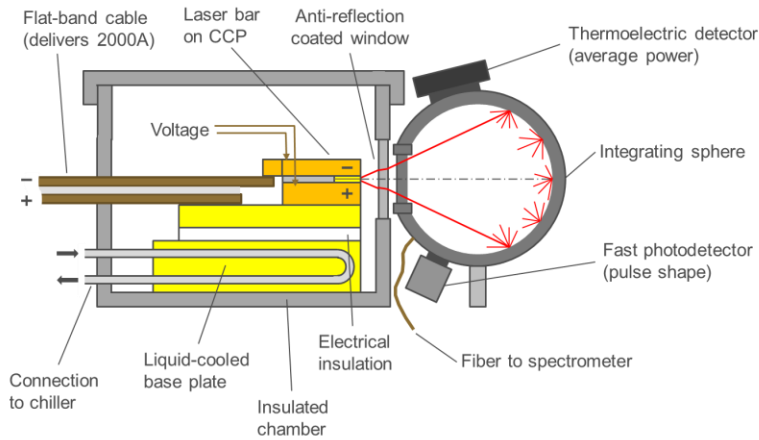Fig. 19: Schematic drawing of low temperature measurement station. An insulated chamber with a window is used to prevent condensation.

Fig. 20: Photo of insulated chamber and integrating sphere with installed single emitter.
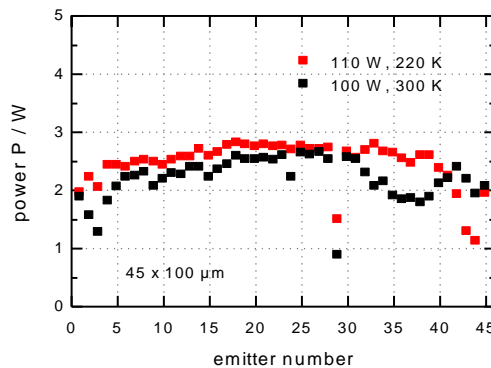

Fig. 21: Power distribution across an example diode laser bar operating at $\lambda = 975$ nm at $T_{HS} = 300$ K (black) and 220 K (red) ($\tau = 1.2$ ms, $\nu = 10$ Hz).

14

The second test station was used to study the optical beam parameters of the diodes, such as near field and far field profiles and the beam parameter product (M^2). A telescopic lens set-up imaged the front facet of the diode onto a CCD-chip, to determine the near field. Moving the chip along the beam axis allowed far field and M^2 to be determined. Measurements of near field with a polarization filter in the beam path gave information on the stress field within the laser bar, by determining the relative power in TE / TM direction. Only small degradation in polarization purity was observed [6] at low temperatures. A more detailed description of the two test stations and their calibration is given in [6] and an example measured power distribution for a laser bar is shown in Fig. 21. In this case, the near field uniformity improved at low temperatures, attributed to the increased efficiency (lower self-heating).

C4.2 Measurements It. 1

In wafer process It. 1, several vertical designs taken from previous research projects were assessed that used vertical waveguide designs with high x ($Al_xGa_{1-x}As$), where high performance at room temperature with $\lambda = 975$ nm was targeted. Laser bars were mounted and tested up to 2 kA. The highest performing bars had a cavity length of 6 mm and a fill factor of 72%, and were packaged with n-side contact via Cu-foil (best available packaging). Record results from a single bar were achieved with an output power of 1.5 kW at 2 kA and $T_{HS} = 300$ K under the relevant pumping conditions for Yb:YAG ($\tau = 1.2$ ms, $\nu = 10$ Hz), as shown in Fig. 22 [3]. Efficiency at 1.5 kW was only 36%, strongly limited by the package resistance of the Cu-foil. When the temperature was reduced to 225 K, the output power increased slightly to 1.7 kW [6]. However, efficiency at high power was not improved due to the increased series resistance at low temperatures.
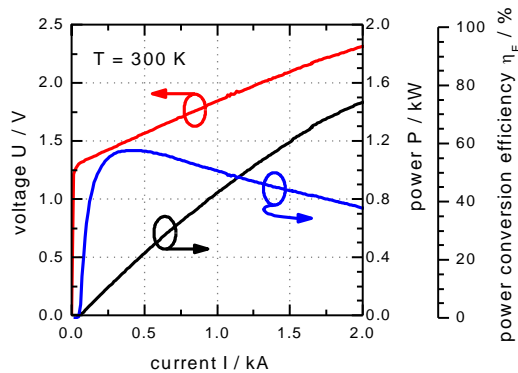

Fig. 22: Voltage (red), power (black) and efficiency (blue) vs. current for a bar from It.1 using a Cu-foil establishing the n-side contact.

C4.3 Short loop process 1

In the first short loop iteration, the Al-content was varied in a 2.4 µm waveguide (see WP2). Single emitters were facet coated (without passivation) and mounted p-side up onto submounts for testing. The optical and electrical performance was studied at different temperatures and the characteristic parameters (threshold current, I_{th}, external differential efficiency $\eta_d = S / (hc/e\lambda)$ and series resistance, R_S) were extracted, as shown in Fig. 23, with the device packaging shown in Fig. 24. A clear trend was observed: at room temperature, low Al-contents led to a significant deterioration in the power characteristic (increasing I_{th}, decreasing η_d) while series resistance decreased (as expected from WP1). As temperature was decreased, the discrepancy in I_{th} and η_d between low and high Al-content designs diminished with universal values of I_{th} and η_d expected at 200 K for Al-contents down to 4% in the waveguide. Simultaneously, series resistance was halved in 4% Al-content designs compared to room temperature optimized designs with 15% Al in the waveguide. However, as discussed in [19] and seen in Fig. 4, the

15

resistance remains much higher than predicted from the properties of the bulk layers, attributed to challenges with carrier injection into the active region.

<u>C4.4 Measurements It. 2</u>

The most promising epitaxial layer designs from short loop process 1 were fabricated into full high-power compatible laser bars in wafer process It. 2. Based on feedback from project partners Lawrence Livermore National Labs, the resonator length was reduced to $L = 4$ mm, to enable a clear benefit in terms of diode laser cost in €/W (fabrication cost increases rapidly with resonator length).

First, the most promising design for cryogenic temperatures featuring low (4%) Al-content waveguides and a single quantum well emitting at $\lambda = 975$ nm were assembled using a Cu-foil to connect the n-side. These bars were tested at $T_{HS} = 203$ K up to a current of 2 kA and achieved 1.5 kW with $\eta_E = 39\%$. The duty cycle had to be reduced to 0.2% (from 1.2%) as the chiller could not sustain the low temperatures at higher duty cycles and high powers. Up to a current of 1 kA however, there was no difference to be seen in power between the two measurements with different duty cycles. Subsequently bars with the same design were assembled using packaging with a massive n-contact, increasing output power to 1.7 kW with $\eta_E = 53\%$ at 1.5 kW (see Fig. 16). This experimentally demonstrated the importance of a low-resistance assembly for high efficiency devices and all further bars were mounted with a massive n-contact.
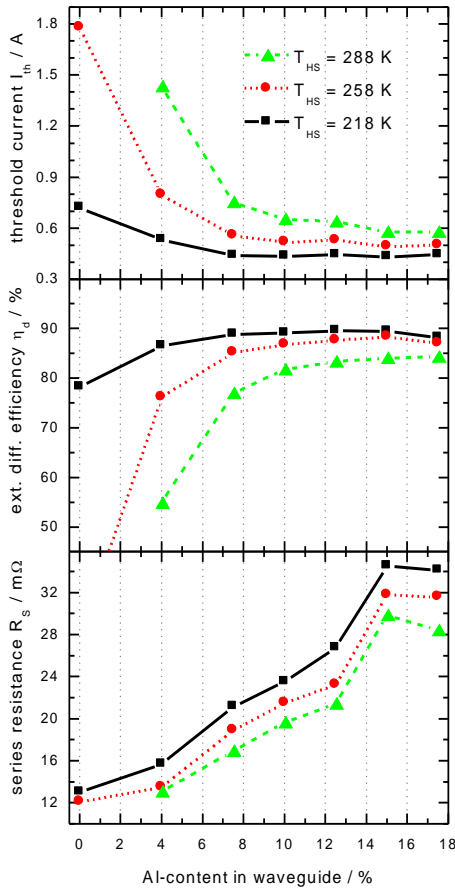

Fig. 23: Threshold current (top), external differential efficiency (middle) and series resistance (bottom) vs. Al-content in the waveguide for three temperatures (288 K – green, 258 K – red, 218 K – black).

Fig. 24: Picture of a single emitter mounted on a CuW heatsink (screening submount).

However, even when improved packaging was used, saturation in the power characteristic was observed starting at 1 kA, limiting output power and efficiency. Bars with the same geometry, epitaxial structure and mounting but using a double instead of a single quantum well showed an increased performance at high bias due to reduced power saturation. Output power increased to 2 kW at 2 kA and $T_{HS} = 200$ K, a record value for a 1-cm wide bar [10]. Efficiency was 61% at 1.5 kW and remained high up to 2 kW (55%) with a spectrum at 2 kW close

to $\lambda = 940$ nm, as shown in Fig. 25. In addition, a modified active region design was tested (all other factors remaining unchanged), seeking to reduce the excess resistance associated with carrier injection. Lower resistance was observed, dropping from 270 µΩ to 230 µΩ, closer to the

predicted electrical resistance of the bulk layers of 160 µΩ, supporting the conclusion that the active region contributes significantly to the electrical resistance, as discussed in [20].
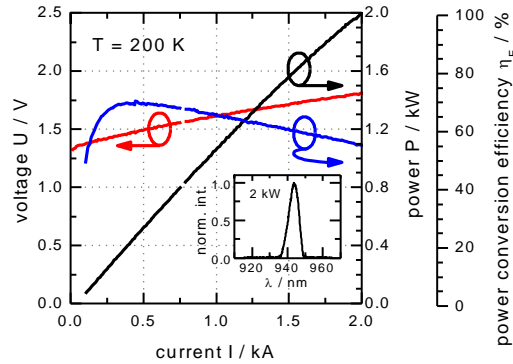

Fig. 25: Voltage (red), power (black) and efficiency (blue) vs. current for a bar emitting at λ = 940 nm from It. 2 using a massive n-side contact (τ = 0.2 ms, ν = 10 Hz) [10].

C4.5 Short loop process 2

The designs from the second short loop process were mounted and tested as single emitters, to select the highest performing design for processing into full 1-cm bars. These designs assessed the benefit of thinner waveguides with increased asymmetry, for lasers operating at λ = 940 nm and at λ = 870 nm at T_{HS} = 200 K. As noted in WP2, various materials were tested as alternative active regions (quantum wells) for operation at λ = 870 nm, with the highest performance option selected. However, although the λ = 870 nm design operated with low threshold, high slope and low resistance, high current testing of full laser structures at T_{HS} = 200 K revealed that a higher order vertical mode was excited, limiting peak achievable output power and efficiency, as shown in Fig. 26. A careful selection of front facet reflectivity and coating thickness was used to suppress the higher order mode, enabling single emitters test samples from the short loop process to operate with close to 70% efficiency at T_{HS} = 200 K, also shown in Fig. 26. The same coating design (with 2% front facet reflectivity) was subsequently used on high power laser bars.
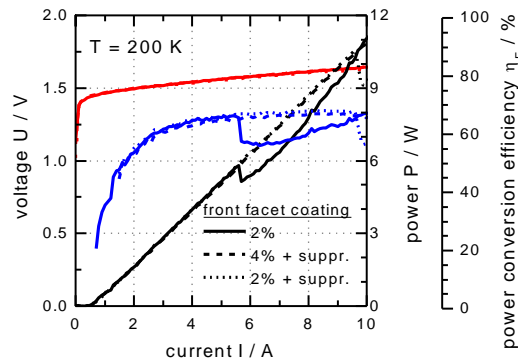
Fig. 26: Voltage (red), power (black) and efficiency (blue) vs. current for single emitters at λ = 870 nm at T_{HS} = 200 K with various front facet coatings (solid – 2% reflectivity, dashed – 4% with higher order mode suppression, dotted - 2% with higher order mode suppression).

C4.6 Measurements It. 3

It.3 included three different epitaxial designs, selected based on their performance in short-loop testing. The same lateral processing and bar packaging was used as in It. 2, with results presented here for bars with 37 x 186 µm stripes. First, a design tailored for low temperature operation with λ = 940 nm was tested, that used low aluminum content in the waveguide. Bars

17

with this design reached record results for peak efficiency (77%) as well as efficiency at 1 kW (70%), as shown in Fig. 27. Second, a λ = 870 nm structure was tested, following the design shown in Fig. 26. Although the facet coating was carefully chosen to inhibit higher order modes (based on short loop process 2), these were not fully eliminated. At T_{HS} = 200 K, a higher-order vertical mode was excited above 200 A, strongly deteriorating power and efficiency. At T_{HS} = 290 K however, the higher order mode was first excited for currents > 800 A, allowing record values for diode laser bars operating around λ = 900 nm to be achieved, namely peak efficiency of 70% and conversion efficiency at 1 kW of 60% [17]. Finally, a further λ = 970 nm structure was tested, with aluminum content suitable for best performance at room temperature. These bars delivered 1 kW output power with an efficiency of 63% at T_{HS} = 290 K. These bars were sent to our project partners at STFC and were subsequently measured at the HiLASE laser facility, which confirmed the results [18], as shown in Fig. 29.

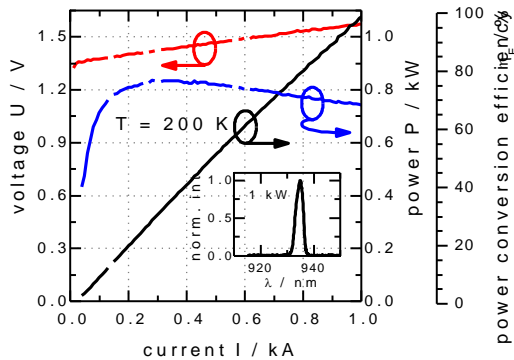

Fig. 27: Voltage (red), power (black) and efficiency (blue) vs. current at T_{HS} = 200 K for an lt. 3 bar operating close to λ = 940 nm (τ = 1.2 ms, ν = 10 Hz)..

Fig. 28: Voltage (red), power (black) and efficiency (blue) vs. current at T_{HS} = 290 K for an lt. 3 bar operating at λ = 900 nm (τ = 0.2 ms, ν = 10 Hz).
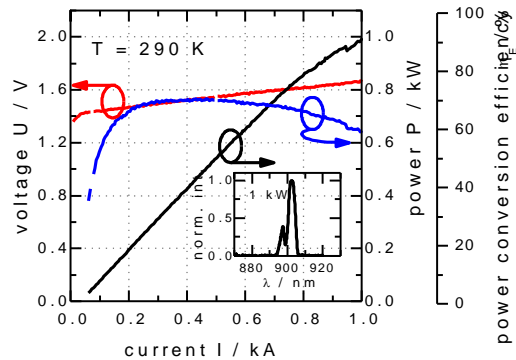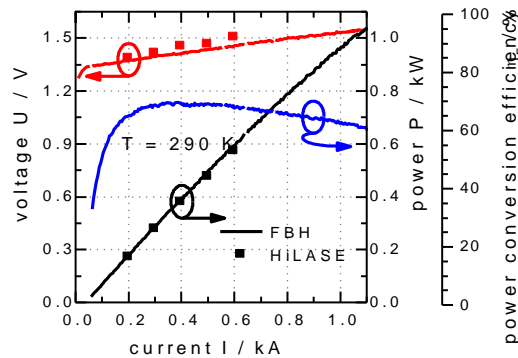

Fig. 29: Voltage (red), power (black) and efficiency (blue) vs. current at T_{HS} = 290 K for an lt. 3 bar operating at λ = 940 nm (τ = 1.2 ms, ν = 10 Hz). Measurements at HiLASE confirm the results.

C4.7 Overall performance progress and prospects for further improvement

The overall performance progress within CryoLaser is summarized in the table below, focusing on performance at an emission wavelength of λ = 940 nm for bars with L = 4 mm. Low temperature operation around T_{HS} = 200 K and the use of custom epitaxial, process and packaging designs enables efficiency at 400 W to be increased to 77%, the highest efficiency ever reported from a laser bar. Also, conversion efficiency similar to the best commercial bars of 70% can be achieved at a much higher power level per bar of 1000 W. Finally, operation power of 1600 W has been confirmed with conversion efficiency of 60% and up to 2000 W

18

demonstrated (limited by available current). Although below the project targets, this represents substantial performance improvement over state of the art, and is expected to enable a large reduction in cost in €/W of the diode laser pump sources for large laser facilities. In addition, important new understanding on the limits to conversion efficiency in diode lasers has been obtained, with significant excess electrical resistance being due to injection into the active region. The improved efficiency seen at low temperatures is largely due to improved slope, caused by increased internal differential efficiency, regulated via the transparency current density. Although both diode lasers with monolithically integrated gratings and high density stacks were fabricated, both showed reduced efficiency and require more technological development. Further increased operating efficiency to > 80% may be achievable if the additional electrical resistance from the active region can be eliminated and if the transparency current can be reduced to around 55 A/cm^2, enabling the highest internal differential efficiency (by improvements to material quality or by operation at even lower temperature).

Parameter	State of art		Results from CryoLaser			Target	Unit
	2011	2015	@ Peak Efficiency	1000 W	1600 W		
Bar width	1	1	1	1	1		cm
Bar thickness	0.015	0.015	0.015	0.015	0.015		cm
Opt. Output Power	200	400	400	1000	1600		W
Opt. Intensity	13	27	27	67	107	107	kW/cm^2
Conversion efficiency	60	70	77	70	60	> 80	%
Operation Temp.	300	300	200	200	200	200	K
Internal grating	No	No	No	No	No	Yes	

D: EXPLOITATION OF RESULTS

D1: Relevance, research status, possible applications and follow-on projects

CryoLaser has had significant impact on the diode laser and high energy class laser research communities and results and technology developed have been actively exploited by the FBH's industrial partners. The strong scientific impact is shown by the 20 publications and conference presentations, 8 of which were invited, including invited talks and tutorials at world leading industrial (SPIE Photonics West) and scientific conferences (CLEO US), with one conference paper selected as a "hot topic" at CLEO US in 2013. Joint papers were presented with DILAS, Lastronics, and Jenoptik that discussed the packaging and diode laser developments necessary to make kW-class QCW laser bars commercially available [8,14,15,16,17] at 940 nm and 870 nm, confirming the rapid industrial take-up of the technology developed within CryoLaser. As noted most recently in [17], kW-class QCW laser bars are for the first time a lower cost pump source in €/W than flash lamps, potentially enabling large market take up as pump sources for commercial pulsed solid state laser systems. High power diode laser bars are also of very strong interest to the research community studying high energy class laser systems, up to and including potential power generation via laser-induced fusion, reflected by the multiple invited talks at the leading conference in this field [1,8,12] and the joint papers with key user groups at HILASE and STFC [7,13,15,16]. One publically funded follow-on project "Doppelpump" is currently active at the FBH as are several industrial collaborations. Further grant applications and collaborations are in active discussion.

D2: Cooperation with partners

CryoLaser collaborated with Lawrence Livermore Labs in the USA and STFC in the UK, meeting regularly at international conferences to discuss status and next steps on the diode laser development for high energy class laser systems. Sample bars were shipped to both LLNL and STFC, who provided feedback on the performance. A scientist from STFC visited the FBH to supervise measurements of high power bars. Lacking the measurement capabilities, STFC in turn sent the delivered bars to their collaborators at the HiLASE facility in the Czech Republic for room temperature characterization, as seen in Fig. 29 and Refs. [13, 15, 16]. The FBH provided valuable guidance on power measurement and also hosted a PhD student from HiLASE, who performed a series of measurements at the FBH facility [7].

D3: Qualifications

One master and two bachelor students completed their studies based on results from CryoLaser, with one PhD thesis planned for completion in 2016.

[A] Michael Sintschuk (Bachelor thesis) "Bestimmung der elektro-optischen Eigenschaften von $Al_xGa_{1-x}As$ in Abhängigkeit von Zusammensetzung und Dotierung," Beuth Hochschule für Technik, Berlin (2014).

[B] Sebastian Dähn (Bachelor thesis) "Untersuchung von High-Density-Stacks unterschiedlicher Montage," Hochschule für Technik und Wirtschaft Berlin (2013).

[C] Hannes Hösler (Masters' thesis) "Untersuchung der Strahleigenschaften von Hochleistungs-Diodenlasern in einem Temperaturbereich von +25°C bis zu -55°C," Ernst-Abbe Fachhochschule Jena, Fachbereich Scitec (2014).

[D] Carlo Frevert (PhD thesis) "High power and high efficiency diode lasers optimized for low temperature operation," Tech. Uni. Berlin (2016, planned).

D4: List of publications and press releases

D4.1 Publications

1. P. Crump, C. Frevert, H. Wenzel, G. Erbert and G. Tränkle, "CryoLaser: Innovative cryogenic diode laser bars optimized for emerging ultra-high power laser applications" (Invited), HEC-DPSSL laser conference, Lake Tahoe, CA, USA (2012).
2. C. Frevert, P. Crump, H. Wenzel, S. Knigge, F. Bugge and G. Erbert, "Efficiency optimization of high power diode lasers at low temperatures", CLEO Europe, CL-P.28-MON (2013).
3. P. Crump, "CryoLaser: Innovative Cryogenic Diode Laser Bars Optimized for Emerging Ultra-high Power Laser Applications," CLEO US, JW1J.2 (2013).
4. P. Crump, G. Erbert, H. Wenzel, C. Frevert, C.M. Schultz, K.-H. Hasler, R. Staske, B. Sumpf, A. Maaßdorf, F. Bugge, S. Knigge, and G. Tränkle "Efficient High-Power Laser Diodes" (Invited), IEEE J. Sel. Top. Quantum Electron., vol. 19, no. 4, pp. 1501211 (2013).
5. C. Frevert, P. Crump, F. Bugge, S. Knigge and G. Erbert, "Study of Waveguide Design for high-power 9xx nm Diode Lasers operating at 200 K", Proc. SPIE, vol. 8965, 89650O (2014).
6. P. Crump , C. Frevert, H. Hösler, F. Bugge, S. Knigge, W. Pittroff, G. Erbert, and G. Tränkle, "Cryogenic ultra-high power infra-red diode laser bars" (Invited), Proc. SPIE, vol. 9002, 90021I (2014).

7. J. Pilar, P. Sikocinski, A. Pranowicz, M. Divoky, P. Crump, R. Staske, A. Lucianetti, and T. Mocek, "Characterization of diode-laser stacks for High-Energy-Class Solid-State Lasers," Proc. SPIE, vol. 8965, Photonics West, San Francisco, USA, Feb. 1-6, 896516 (2014).
8. P. Crump, T. Toepfer, and J. Neukum, "1kW peak power operation of conduction cooled 940nm single bars, for use as pump source in Peta-Watt applications" (Invited), HEC-DPSSL laser conference, Oxford, UK (2014).
9. H. Wenzel, K.H. Hasler, C. Frevert, P. Crump and G. Erbert, "Simulation of high-power semiconductor lasers at sub-zero Temperatures", AMaSiS workshop, WIAS Berlin (2015).
10. C. Frevert, P. Crump, F. Bugge, S. Knigge, A. Ginolas, and G. Erbert, "Low-temperature Optimized 940 nm Diode Laser Bars with 1.98 kW Peak Power at 203 K", CLEO US, SM3F.8 (2015).
11. P. Crump, C. Frevert, G. Erbert, and G. Tränkle, "High Power Diode Lasers for Pumping High Energy Solid State Lasers" (Invited tutorial), CLEO US, SM3M.1 (2015).
12. C. Frevert, F. Bugge, S. Knigge, A. Ginolas, G. Erbert, and P. Crump, "Progress in development of kW-class diode laser bars for pump applications within the CryoLaser project" (Invited), HEC-DPSSL laser conference, Stirin, Czech Republic (2015).
13. A. Lucianetti, J. Pilar, A. Pranovich, M. Divoky, T. Mocek, K. Ertel, H. Jelinkov, P. Crump, C. Frevert, R. Staske, G. Erbert, and G. Tränkle "Assessment of high-power kW-class single-diode bars for use in highly efficient pulsed solid-state laser systems" Proc. SPIE 9348, Photonics West, San Francisco, USA, Feb. 07-12, 934811 (2015).
14. P. Crump, C. Frevert, F. Bugge, S. Knigge, G. Erbert, G. Tränkle, A. Pietrzak, R. Hülsewede, M. Zorn, J. Sebastian, J. Lotz, W. Fassbender, J. Neukum, J. Körner, J. Hein and T. Töpfer, "Progress in high-energy-class diode laser pump sources" Proc. SPIE 9348, Photonics West, San Francisco, USA, Feb. 07-12, 93480U (2015).
15. P. Crump, C. Frevert, A. Ginolas, A. Knigge, A. Maassdorf, J. Lotz, W. Fassbender, J. Neukum, J. Korner, T. Topfer, A. Pranovich, M. Divoky, A. Lucianetti, T. Mocek, K. Ertel, M. De Vido, G. Erbert, and G. Trankle, "Joule-Class 940-nm Diode Laser Bars for Millisecond Pulse Applications", Phot. Techn. Lett. vol.27, no.15, (2015).
16. P. Crump, C. Frevert, A. Ginolas, S. Knigge, A. Maaßdorf, J. Lotz, W. Fassbender, J. Neukum, J. Körner, T. Töpfer, A. Pranovich, M. Divoky, A. Lucianetti, T. Mocek, K. Ertel, M. De Vido,G. Erbert and G. Tränkle, "Joule-Class 940 nm Diode Laser Bars for Millisecond Pulse Applications", Proc. IEEE Photonics Conf. (IPC 2015), Reston, VA, USA, Oct. 4-8, pp. 555-556 (2015).
17. A. Pietrzak, M. Woelz, R. Huelsewede, M. Zorn, O. Hirsekorn, J. Meusel, A. Kindsvater, M. Schröder, V. Bluemel, J. Sebastian, C. Frevert, F. Bugge, S. Knigge, A. Ginolas, G. Erbert and P. Crump, "Progress in the development of kilowatt-class diode laser bars for pump applications", Proc. ASSL, Paper ATh2A.7 (2015).
18. M. Weyers, C. Frevert, F. Bugge, S. Knigge, A. Ginolas, G. Erbert and P. Crump, "High power and high efficiency from GaAs/AlGaAs laser bars optimized for cryogenic operation" (Invited), NLS-24 (2015).
19. C. Frevert, P. Crump, F. Bugge, S. Knigge and G. Erbert, "The impact of low Al-content waveguides on power and efficiency of 9xx nm diode lasers between 200 and 300 K", Semicond. Sci. Technol. 31 (2016).
20. C. F. Frevert, F. Bugge, S. Knigge, A. Ginolas, G. Erbert and P. Crump, "940nm QCW diode laser bars with 70% efficiency at 1 kW output power at 203K: analysis of remaining limits and path to higher efficiency and power at 200 K and 300 K" (Invited), Proc SPIE 9733-20 (2016).

D4.2 List of press / media releases

Three press releases (one per year) were generated within the CryoLaser project.

● "Energy-sources of the future: novel diode lasers for ultra-high power laser applications" (2013).
www.fbh-berlin.com/fileadmin/downloads/Press/2013/PM_FBH_Cleo_english_2013_06_07.pdf

● "Ultra-high energy laser bars - record performance in frosty environment" (2014).
www.fbh-berlin.com/publications-patents/frequent/05-uv-leds/research-in-focus

● "Diode lasers bars with 2 kW output power for ultra-high power laser applications" (2015).
www.fbh-berlin.com/press/press-releases/detail/diode-lasers-bars-with-2-kw-output-power-for-ultra-high-power-laser-applications

More than 66 press articles have focused on the CryoLaser project. Examples include:

● Leibniz Journal: "Kleines Reiskorn, große Wirkung" (2013)
www.leibniz-gemeinschaft.de/fileadmin/user_upload/downloads/Presse/Journal/04_13_Luft/LeibnizJournal_04_2013_Kleines_Reiskorn_grosse_Wirkung.pdf

● Laser Focus World: "CryoLasers target >80% power conversion efficiency" (2013)
www.laserfocusworld.com/articles/print/volume-49/issue-10/newsbreaks/CryoLasers-target-80-power-conversion-efficiency.html

● Research news on FBH website: "Quasi-continuous-wave diode laser bars with increased power (2 kW) and peak conversion efficiency (77%) at 203 K" (2015)
www.fbh-berlin.com/research/research-news/detail/quasi-continuous-wave-diode-laser-bars-with-increased-power-2nbspkw-and-peak-conversion-efficiency-77-at-203nbspk